The Konus-*Wind* catalog of gamma-ray bursts with known redshifts

I. Bursts detected in the triggered mode

Anastasia Tsvetkova
on behalf of the Konus-*Wind* team
Ioffe Institute, St.Petersburg, Russia

tsvetkova@mail.ioffe.ru

Contents

- Motivation
- The Konus-*Wind* experiment
- The burst sample
- The GRB analysis and results
- Rest-frame hardness-intensity correlations
- Selection effects
- GRB detection horizon
- GRB luminosity and energy release functions
- GRB formation rate
- Summary and conclusion

The talk is based on the paper Tsvetkova, Frederiks, Golenetskii et al., ApJ accepted

Motivation

- ~450 GRBs with reliable *z* by 2016 June (>200 observed by Konus-*Wind*);
- Redshift -> distance, age, rest-frame energetics;
- The unbiased comparison between GRBs;
- Possibility to test GRB models;
- GRBs could probe the properties of high-redshift universe:
  - Cosmic expansion
  - Star formation history at high redshifts
  - Reionization history
  - Metal evolution
  - History of cosmic acceleration
  - Evolution of dark energy

Joint Russian-US Konus-*Wind* experiment

- The Konus-Wind (KW) is aimed primarily at GRB and SGR studies;
- Launched on November 1, 1994: almost 23 years of continuous operation;
- Observation statistics (triggers): 2900 – GRBs (Fermi ~1500,
  BATSE ~2700, Swift ~1150),
  260 – SGRs, 1000 – SFs.

Advantages

- Wide energy band (20 keV–20 MeV);
- Exceptionally stable background;
- The orbit of s/c excepts interferences from radiation belts and the Earth occultation;
- Continuous observations of all sky;
- Duty circle 95%;
- Observes almost all bright events ($>10^{-6}$ erg cm^{-2} s^{-1}).

Two modes:

- Waiting mode: G1, G2, G3 @ 2.944 s resolution;
- Triggered mode:
  LC res. is 2 ms –256 ms, from T_0-0.512 s to T_0+230 s;
  128-ch spectra (20 keV – 20 MeV).
- Two NaI detectors (S1 and S2) are located on opposite faces of spacecraft, observing correspondingly the southern and northern celestial hemispheres;
- ~100-160 cm^2 effective area;
- Now in orbit near L_1, up to 2.1 million km (~7 light s) from Earth;
- Light curves (LCs) in three energy windows: G1 (~20–80 keV, at present), G2 (~80–300 keV), and G3 (~300–1200 keV).

The burst sample

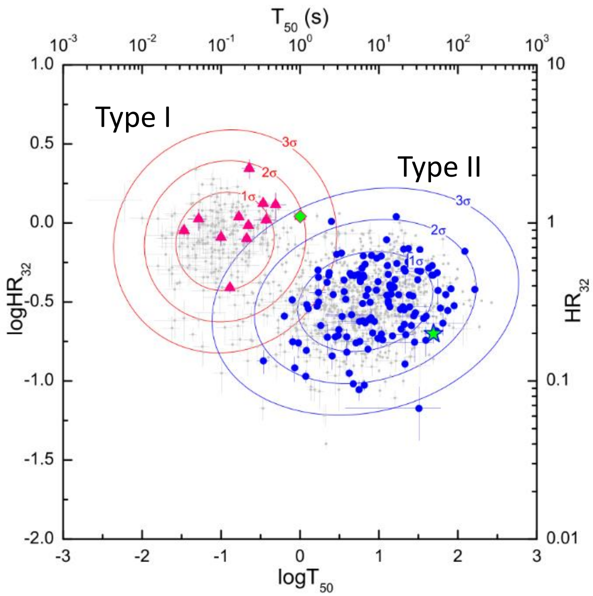

Svinkin et al. (2016)

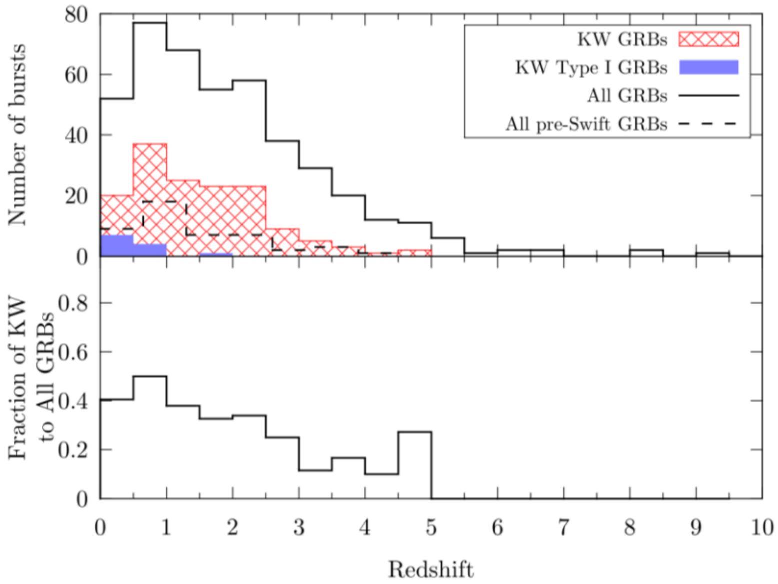

- 150 triggered GRBs (1997 Feb to 2016 Jun);
- $0.1 \leq z \leq 5$;
- 12 Type I (the merger-origin, typically short/hard) GRBs;
- 138 Type II (the collapsar-origin, typically long/soft) GRBs;
- 32 GRBs have reasonably-constrained (from optical/IR afterglow or in two spectral band simultaneously) jet breaks times -> collimation.

Analysis

Durations (T_{100}, T_{90}, T_{50}) + spectral lags

↓

Time intervals for spectral analysis were selected based on T_{100} and PCR

↓

Spectral analysis (CPL & Band models)

↓

Observer-frame energetics (in 10 keV – 10 MeV range)

↓ + Redshift

Rest-frame energetics

↓ + Jet break time

Collimation-corrected energetics

Typical KW light curves

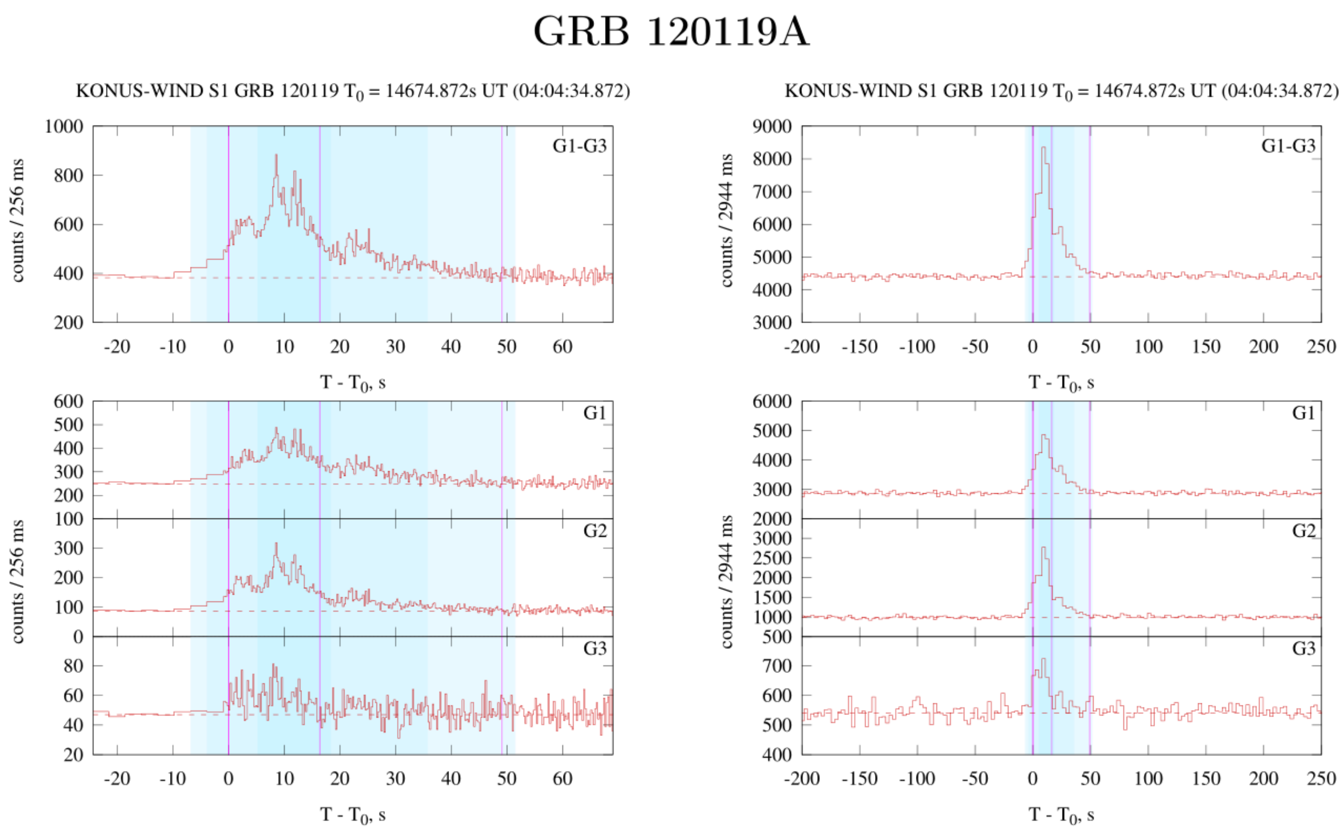

KW trigger (left) and waiting (right) mode light curves.

T_{100} is determined at 5σ excess above background.
The durations were calculated using the counts in the G2+G3 energy band (~80–1200 keV at present).

Durations and spectral lags

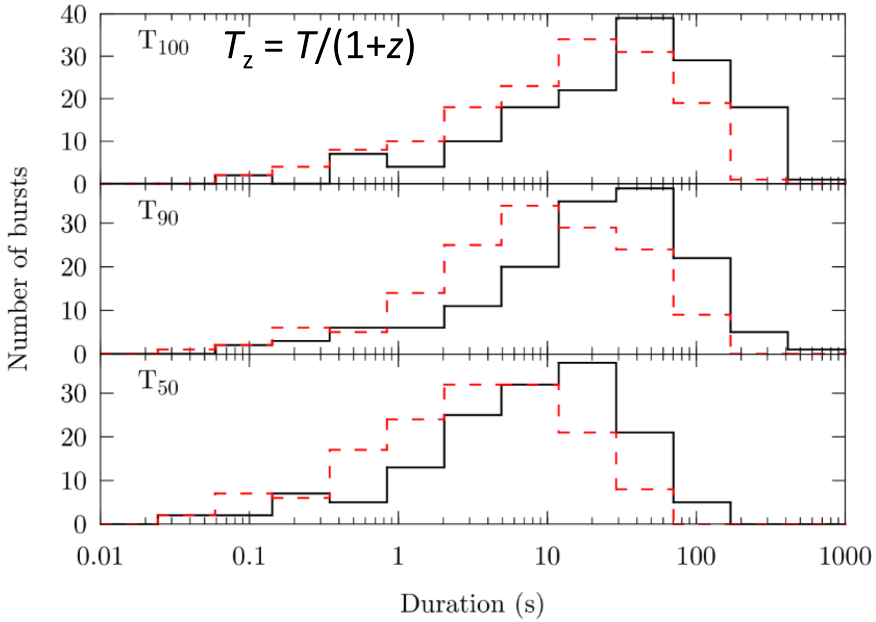

$0.1\ \mathrm{s} < T_{100} < 458$ s, median: 37 s;
$0.07\ \mathrm{s} < T_{90} < 441$ s, median: 22 s;
$0.03\ \mathrm{s} < T_{50} < 167$ s, median: 7.6 s;

$0.08\ \mathrm{s} < T_{z100} < 171$ s, median: 14 s;
$0.05\ \mathrm{s} < T_{z90} < 122$ s, median: 10 s;
$0.025\ \mathrm{s} < T_{z50} < 50$ s, median: 3 s.

For the 58 GRBs selected for the spectral lag analysis, the numbers of lags calculated are as follows: $\tau_{lagG2G1}$ – 55, $\tau_{lagG3G1}$ – 32, $\tau_{lagG3G2}$ – 38.

The observer-frame energy band G2+G3 corresponds to different energy bands in the source-frame thus introducing a variable energy-dependant factor which must be accounted for when analyzing the rest-frame durations and spectral lags.

Parameter Name	Min Value	Max Value	Mean Value	Median Value
$\tau_{lagG2G1}$ (ms)	0.6	2495	292	150
$\tau_{lagG3G1}$ (ms)	4.8	5106	543	343
$\tau_{lagG3G2}$ (ms)	2.1	765	176	132
$\tau_{lagG2G1,z}$ (ms)	0.4	1290	143	68
$\tau_{lagG3G1,z}$ (ms)	3.7	2630	257	133
$\tau_{lagG3G2,z}$ (ms)	1.4	388	85	68

The spectral lag (τ_{lag}) is a quantitative measure of spectral evolution, when the emission in a soft detector band peaks later or has a longer decay relative to a hard band; a positive τ_{lag} corresponds to the delay of the softer emission.

Spectral analysis

- Two types of spectra:
  - Time-integrated (TI) – the interval closest to T_{100};
  - "Peak" – close to the time when the peak count rate (PCR) is reached;
- Two spectral models:
  - CPL: $$f(E) \propto E^{\alpha} \exp\left(-\frac{E(2+\alpha)}{E_p}\right)$$
  - Band function (Band et al., 1993):

$$f(E) \propto \begin{cases} E^{\alpha} \exp\left(-\frac{E(2+\alpha)}{E_p}\right), & E < (\alpha-\beta)\frac{E_p}{2+\alpha} \\ E^{\beta}\left[(\alpha-\beta)\frac{E_p}{(2+\alpha)}\right]^{(\alpha-\beta)} \exp(\beta-\alpha), & E \geq (\alpha-\beta)\frac{E_p}{2+\alpha}, \end{cases}$$

  - PL model (if both "curved" models result in ill-constrained fits): $f(E) \propto E^{\alpha}$
- BEST model: χ^2_{CPL}-χ^2_{Band}>6 ➡ the Band function;
- 20 cnts/channel binning to ensure Gaussian-distributed count statistics.

- Band function is the best fit model for 54 TI (51 peak) spectra of Type II bursts;
- CPL is the best fit model for 83 TI (86 peak) spectra of Type II bursts;
- PL is the best fit model for GRB 080413B (both TI & peak spectra);
- All Type I burst spectra are fitted best by the CPL function.

Typical KW spectra

GRB 070125

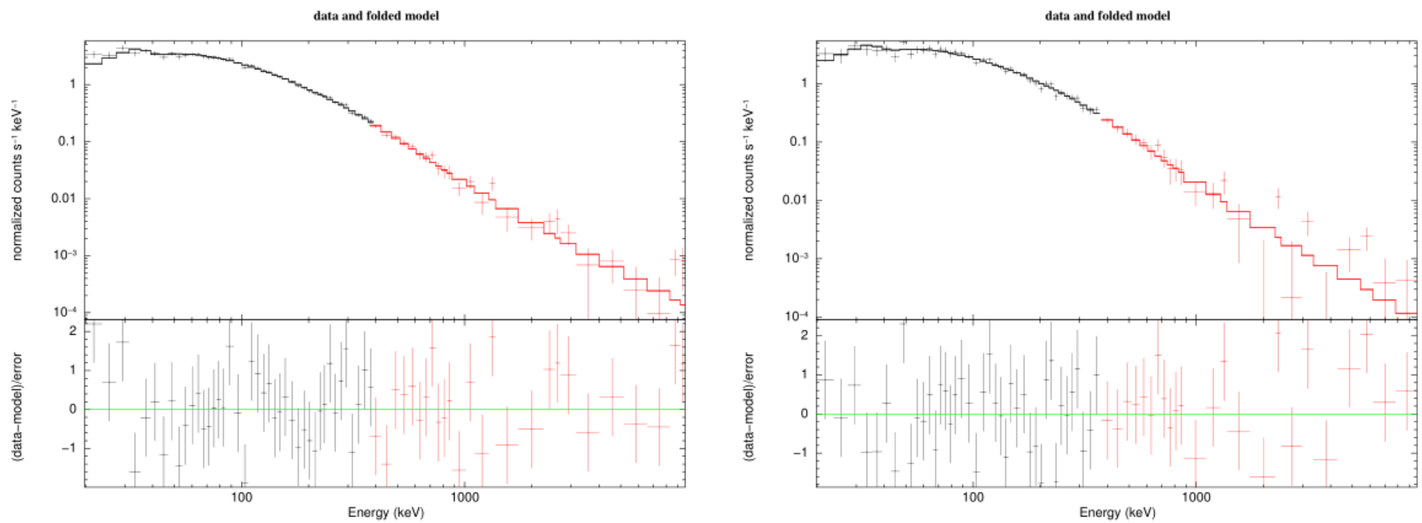

Xspec spectral fits of the time-integrated (left) and the peak (right) spectra.

Fit model parameters

	Spectrum	Accumulation interval	Model	α	β	$E_{\rm p}$ (keV)	F (10^{-6} erg cm^{-2} s^{-1})	χ^2/dof (Prob.)
Best	Time-integrated	0.000–75.008	GRBM	$-1.10^{+0.06}_{-0.05}$	$-2.09^{+0.06}_{-0.08}$	372^{+36}_{-31}	$2.36^{+0.13}_{-0.13}$	88.6/89 (0.49)
	Peak	34.560–50.432	GRBM	$-0.99^{+0.10}_{-0.09}$	$-2.27^{+0.15}_{-0.27}$	370^{+57}_{-47}	$2.50^{+0.24}_{-0.25}$	79.7/88 (0.72)
Good	Time-integrated	0.000–75.008	CPL	$-1.23^{+0.04}_{-0.04}$	−−	518^{+41}_{-35}	$1.71^{+0.07}_{-0.06}$	118.0/90 (0.026)
	Peak	34.560–50.432	CPL	$-1.09^{+0.06}_{-0.06}$	−−	455^{+45}_{-37}	$1.92^{+0.10}_{-0.09}$	86.0/89 (0.57)

Spectral indices

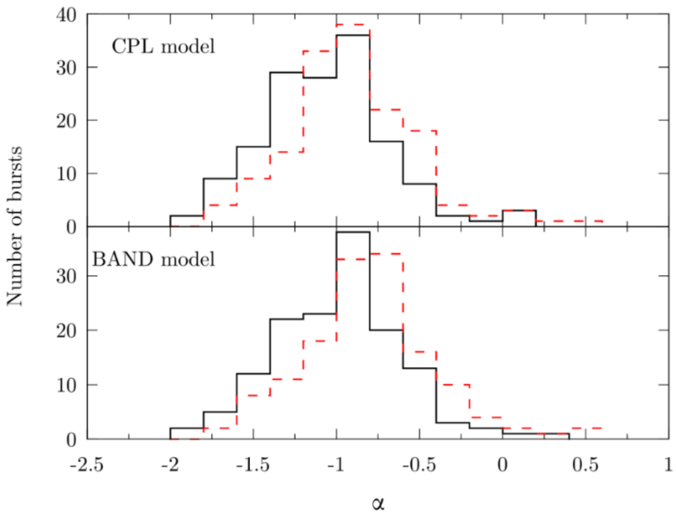

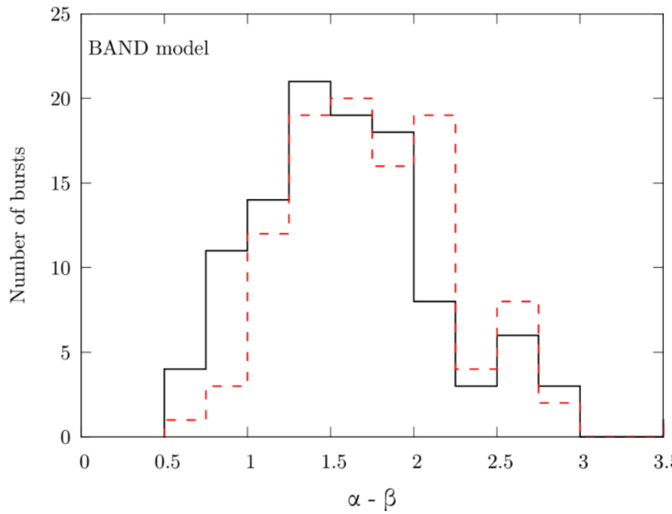

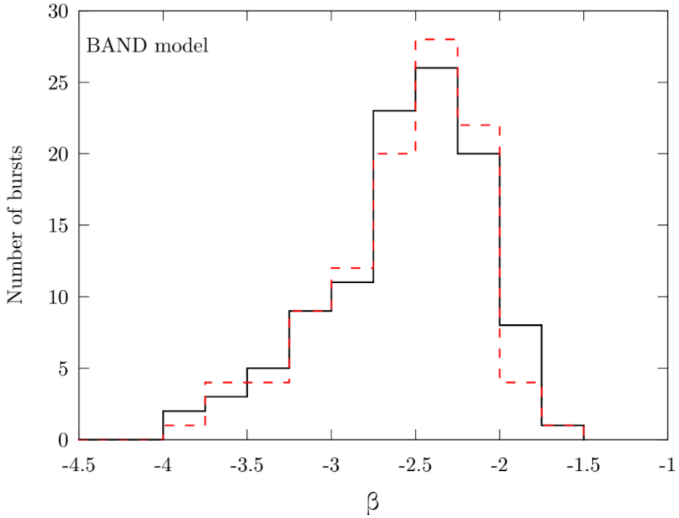

The fraction of the bursts which violate the −2/3 synchrotron line-of-death:
9% (TI sp.) & 21% (peak sp.) of the 68% CL lower limits on α are shallower.
the −3/2 synchrotron cooling limit:
7% (TI sp.) & 3% (peak sp.) of the 68% CL upper limits are steeper.

Peak energies

- E_p for the BEST model varies from ~40 keV to ~3.5 MeV (GRB 090510);
- The TI spectrum E_p distributions for both models peak around 250 keV;
- The peak spectrum E_p distributions peak around 300 keV;
- The corresponding rest-frame $E_{p,z} = (1+z)E_p$ vary from ~50 keV to ~6.7 MeV (GRB 090510);
- The median Ep ≈ 650 keV for Type I GRBs.

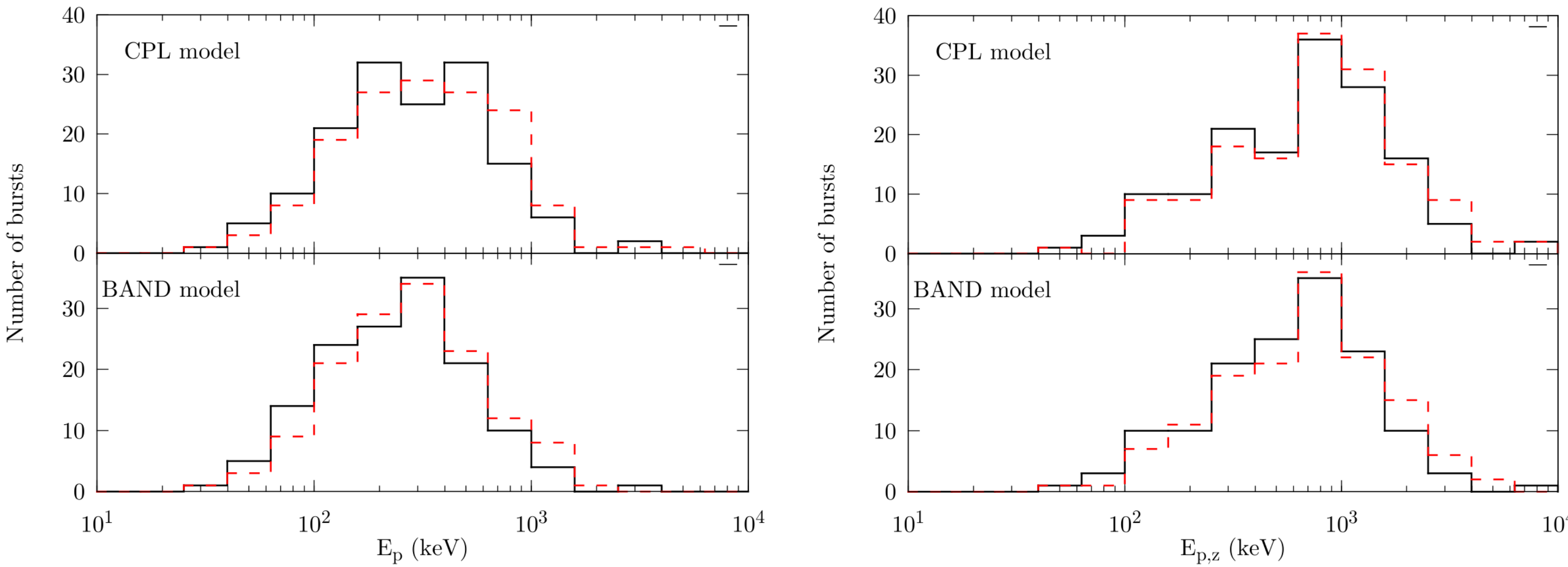

Observer-frame energetics

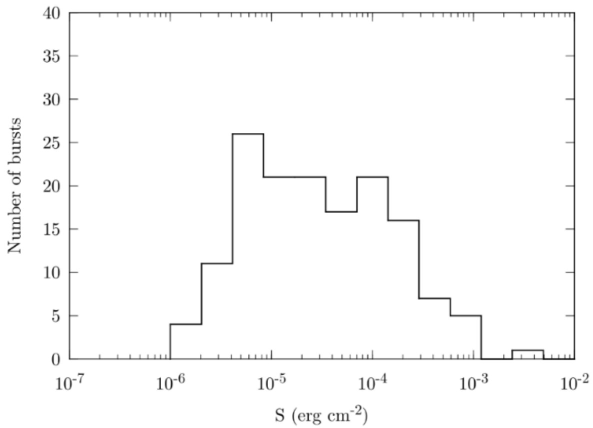

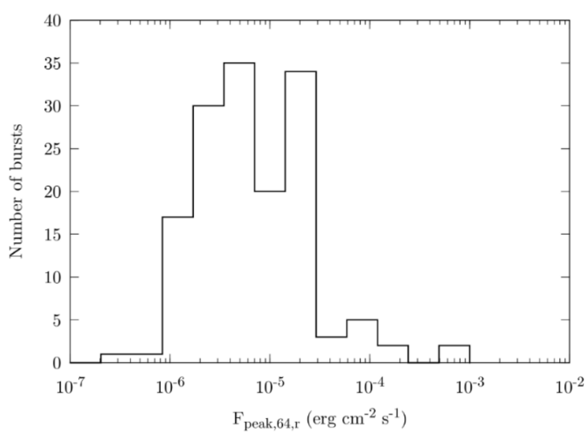

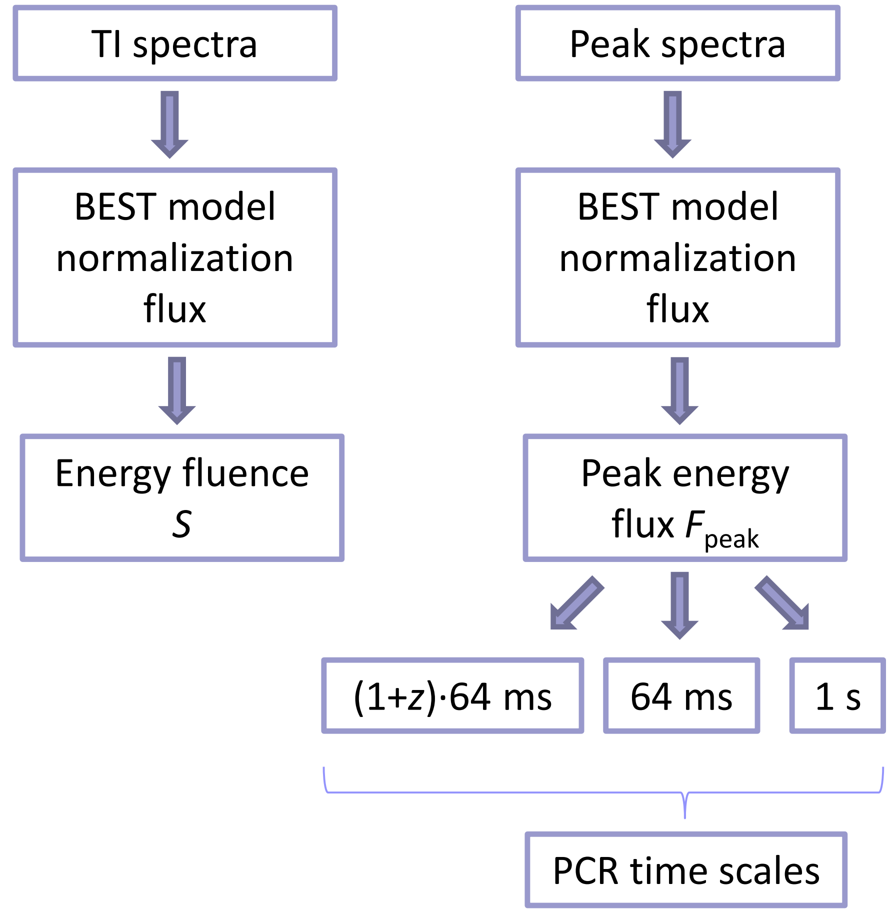

1×10^{-6} erg cm^{-2} < S <2.9×10^{-3} erg cm^{-2} (GRB 130427A)

3×10^{-7} erg cm^{-2}s^{-1} < $F_{peak,64}$ < 9.0×10^{-4} erg cm^{-2}s^{-1} (GRB 110918A)

Rest-frame energetics

The most energetic KW burst:
GRB 090323 (E_{iso} = 5.81 × 10^{54} erg).
The most luminous burst:
GRB 110918A (L_{iso} = 4.65 × 10^{54} erg s^{-1}).

e.g. Bloom et al. (2001) or Kovacs et al. (2011)

$$k = \frac{F[E_1/(1+z), E_2/(1+z)]}{F[e_1, e_2]}$$

e_1 = 10 keV, e_2 = 10 MeV;
E_1 = 1 keV, E_2 = (1+z)·10 MeV

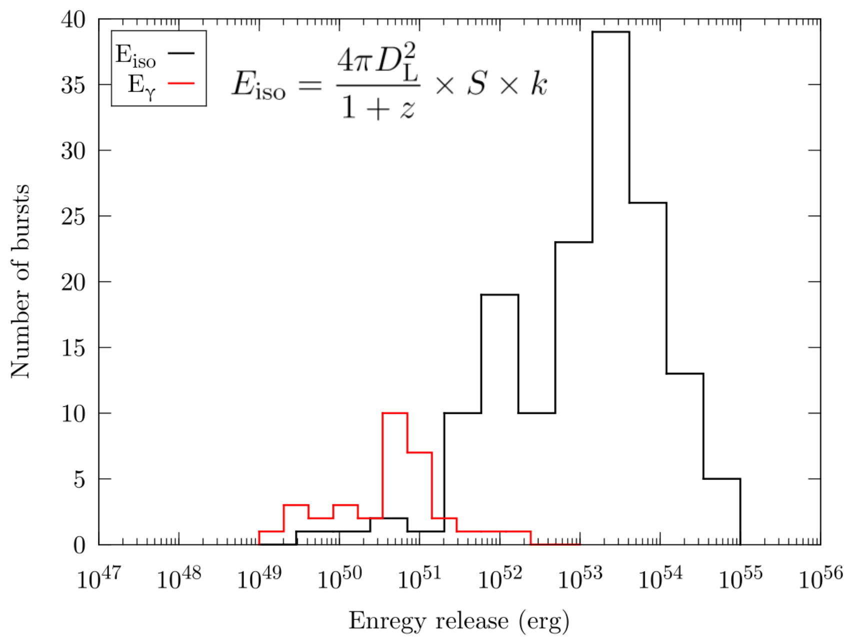

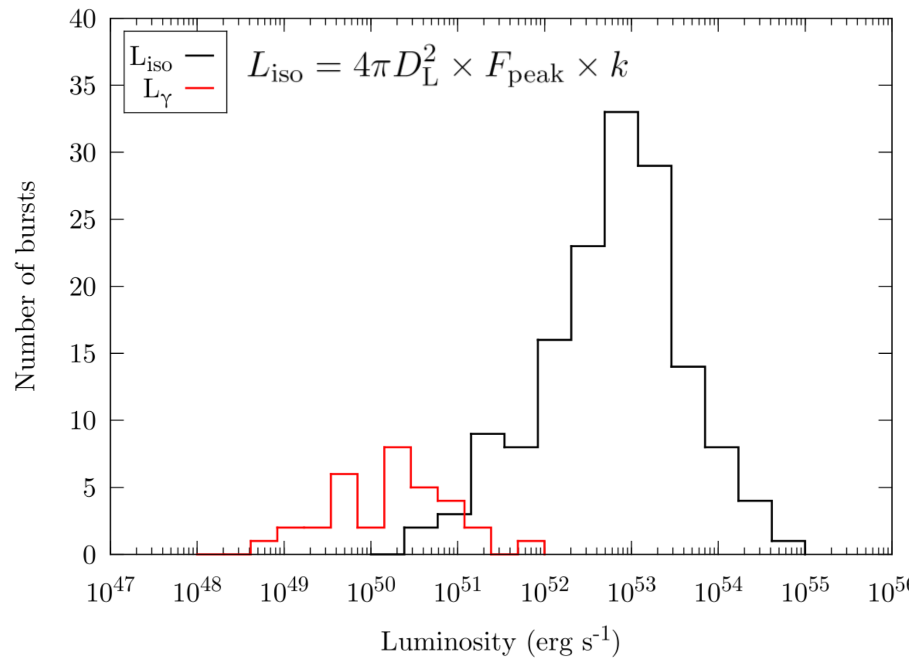

Collimation-corrected rest-frame energetics

32 (2 Type I & 30 Type II) GRBs have reasonably-constrained (from optical/IR afterglow or in two spectral band simultaneously) t_{jet}:
$1.9° < \theta_{jet} < 25.5°$
$5.5\times10^{-4} < 1-\cos\theta_{jet} < 0.098$

The brightest KW GRB in terms of both E_γ and L_γ is GRB 090926A ($E_\gamma \simeq 1.23 \times 10^{52}$ erg, $L_\gamma \simeq 5.50 \times 10^{51}$ erg s^{-1}, $\theta_{jet} \simeq 6.20°$)

CBM with constant number density
Sari et al. (1999)

$$\theta_{\rm jet,HM} = \frac{1}{6}\left(\frac{t_{\rm jet}}{1+z}\right)^{3/8}\left(\frac{n\eta_\gamma}{E_{\rm iso,52}}\right)^{1/8}$$

Stellar-wind-like CBM
Li & Chevalier (2003)

$$\theta_{\rm jet,WM} = 0.2016\left(\frac{t_{\rm jet}}{1+z}\right)^{1/4}\left(\frac{\eta_\gamma A_*}{E_{\rm iso,52}}\right)^{1/4}$$

$$A_* = (\dot{M}_{\rm w}/(4\pi v_{\rm w})/(5\times10^{11}\ {\rm g\ cm^{-1}})$$

$n = 1$ cm^{-3}, $\eta_\gamma = 0.2$, $A_* = 1$

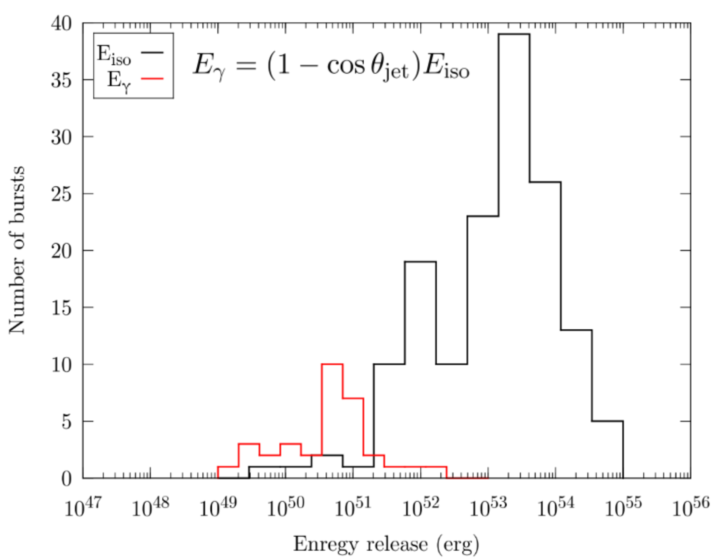

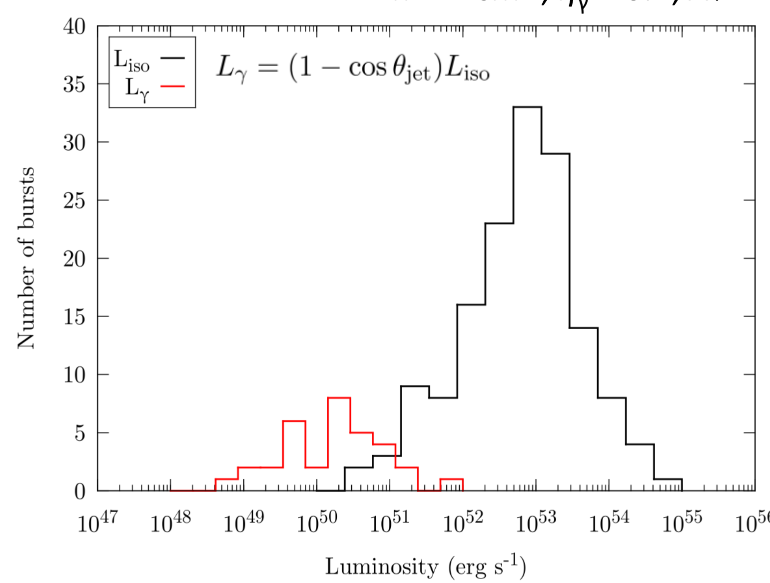

Hardness-duration distribution

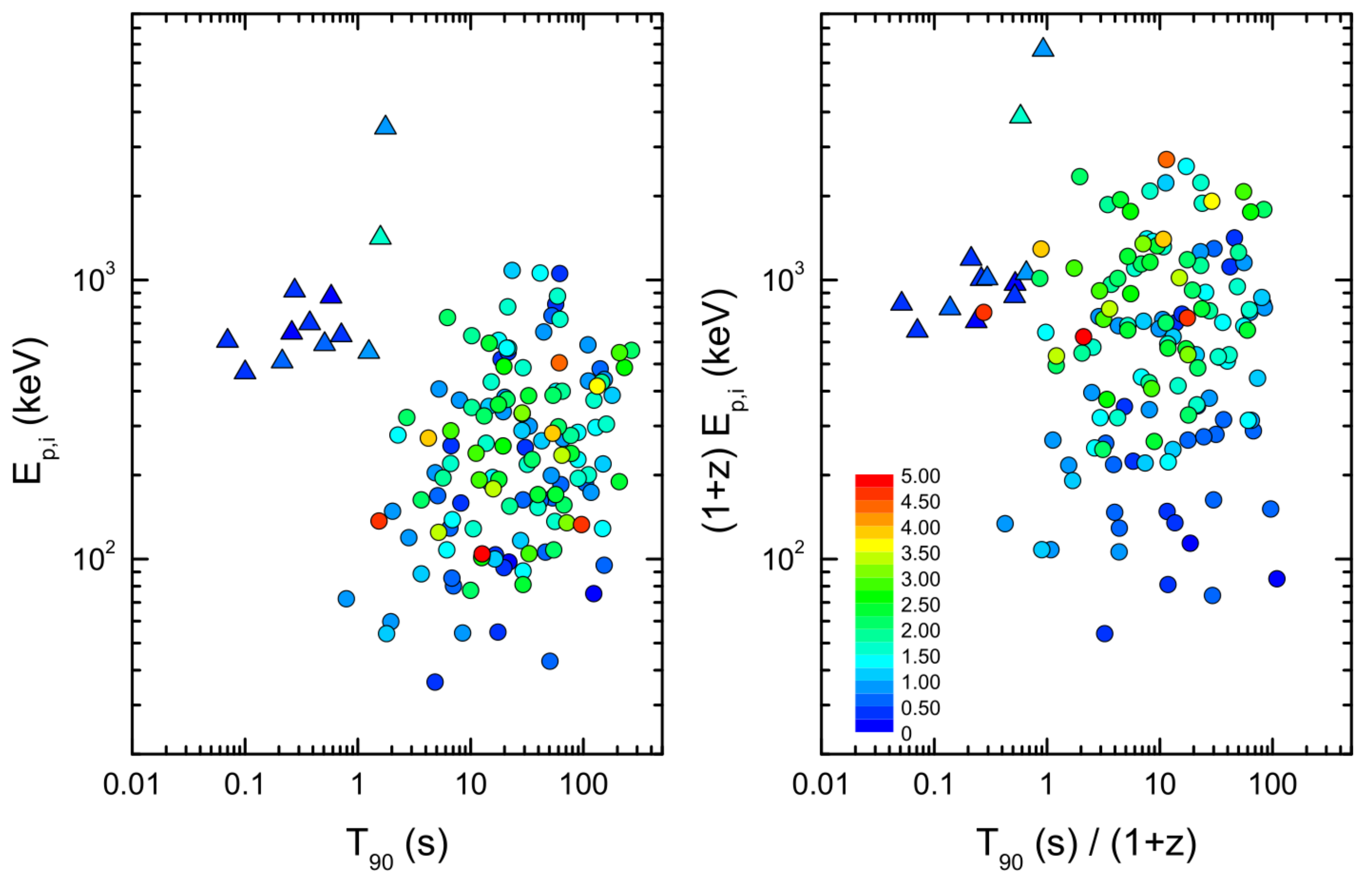

Hardness-duration distribution

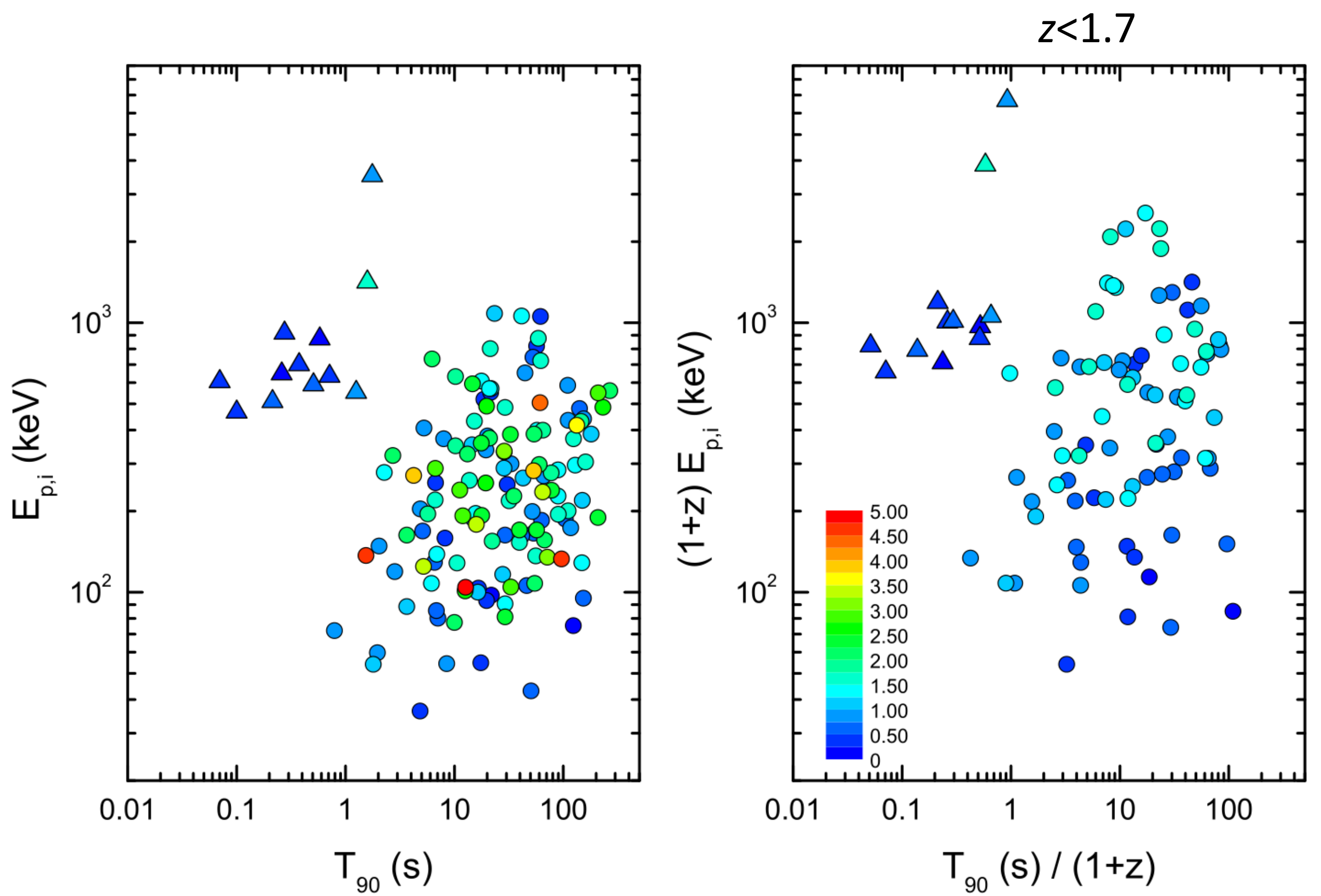

Hardness-intensity correlations

Amati relation
N=137, ρ_S=0.70
P=1.4×10^{-21}
a = 0.469

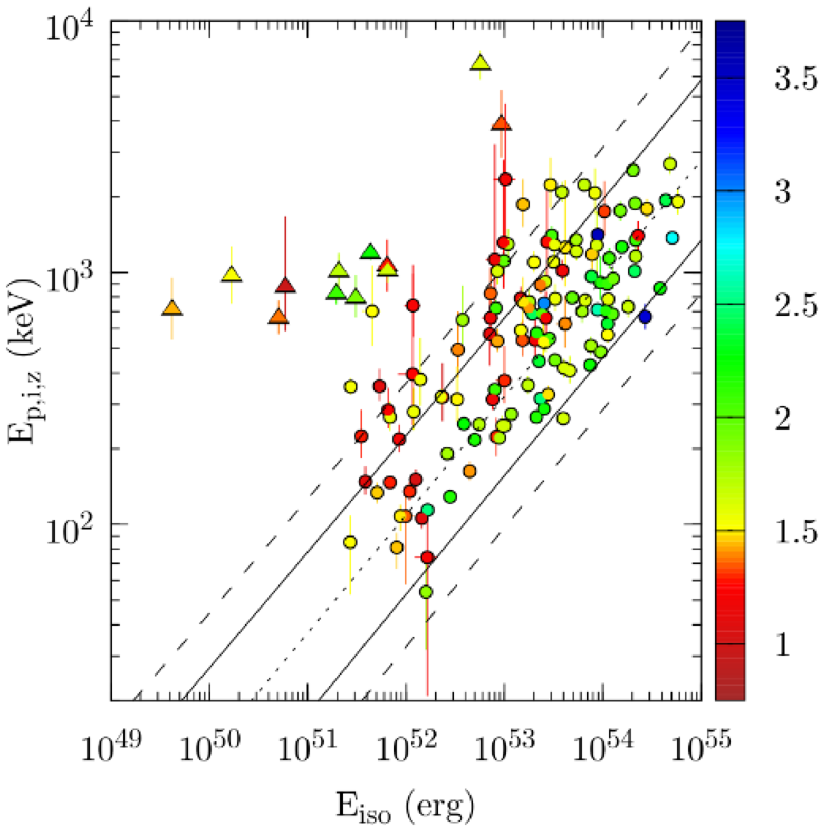

Yonetoku relation
N=136, ρ_S=0.73
P=1.6×10^{-23}
a = 0.494

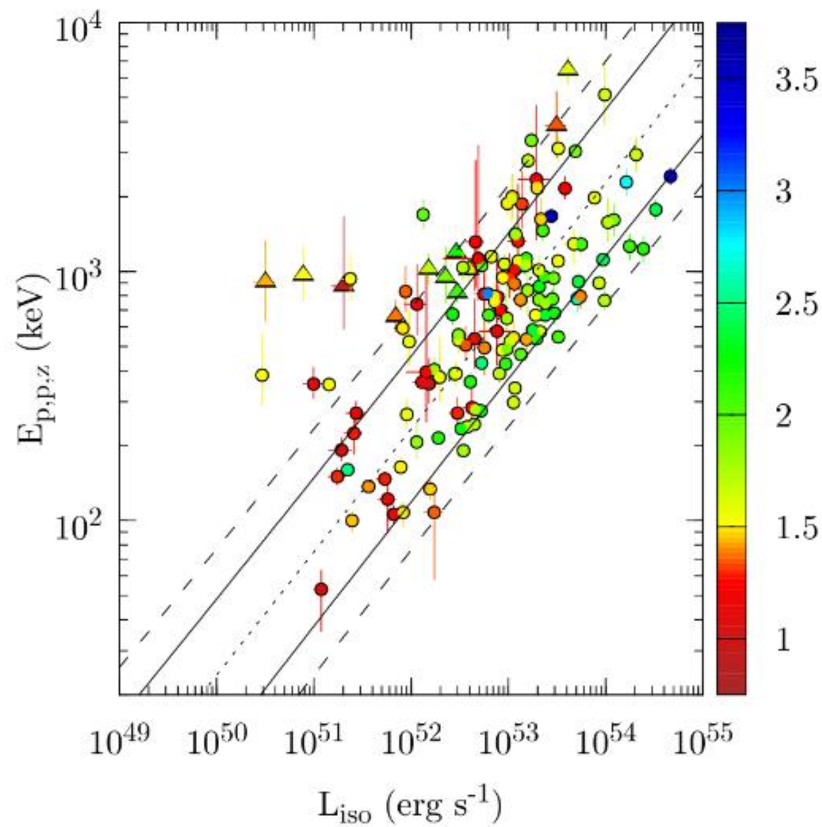

Hardness-intensity correlations

Amati relation
N=137, ρ_S=0.70
P=1.4×10^{-21}
a = 0.469

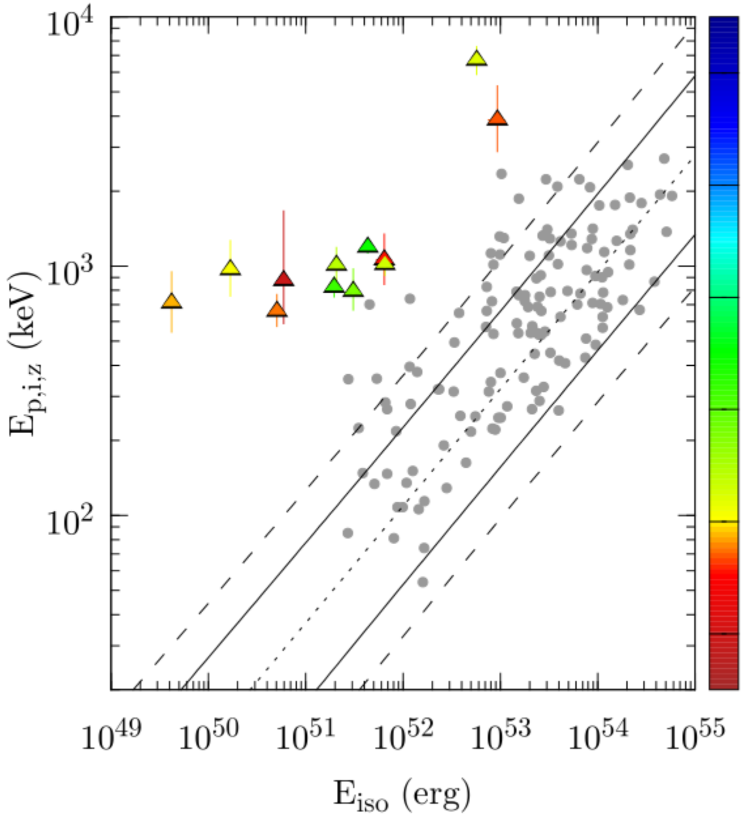

Yonetoku relation
N=136, ρ_S=0.73
P=1.6×10^{-23}
a = 0.494

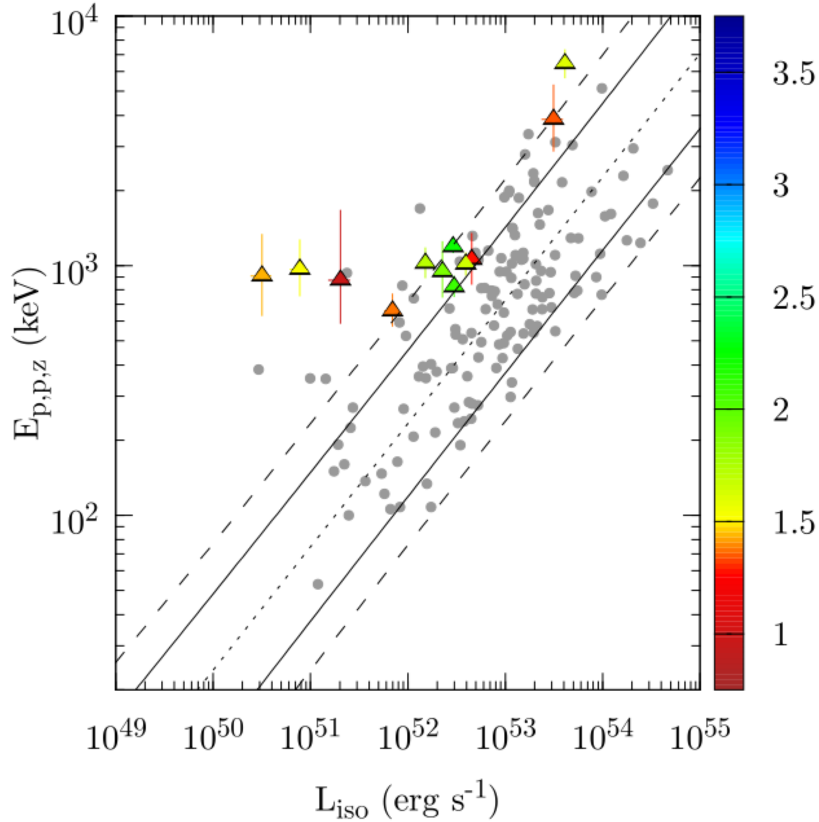

Hardness-intensity correlations

Amati relation
ρ_S=0.80
P=7.2×10^{-8}
a = 0.561

Ghirlanda relation
N=30
ρ_S=0.77
P=4.5×10^{-7}
a = 0.604

Coll.-corrected Yonetoku relation
N=30
ρ_S=0.64
P=9.7×10^{-5}
a = 0.729

Yonetoku relation
ρ_S=0.78
P=2.9×10^{-7}
a = 0.496

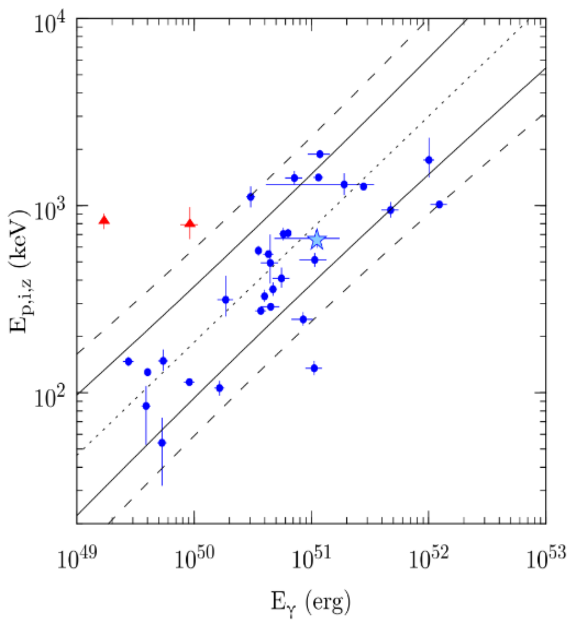

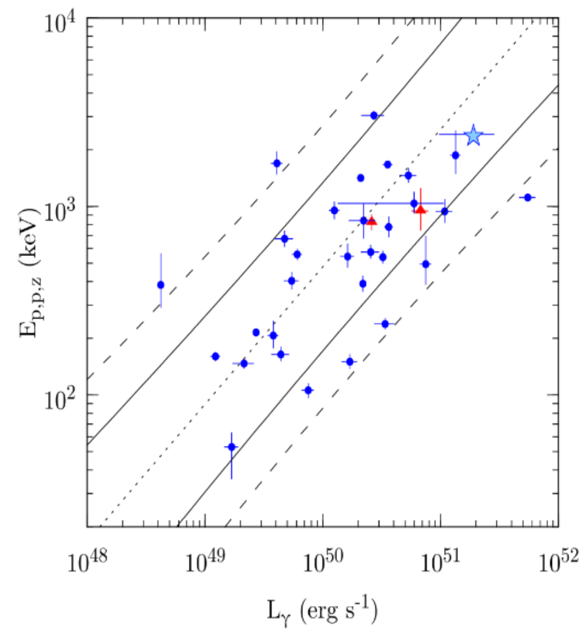

GRB 110918A Frederiks et al. (2013)

Hardness-intensity correlations

Nukers estimate (Tremaine et al. 2002):

$$\chi^2 = \sum_{i=1}^{N} \frac{(y_i - a x_i - b)^2}{a^2 \sigma_{xi}^2 + \sigma_{yi}^2 + \sigma_{\rm int}^2}$$

Correlation	N	ρ_S	P_{ρ_S}	a	b	$a_{\sigma_{\rm int}}$	$b_{\sigma_{\rm int}}$	$\sigma_{\rm int}$
				Type I GRBs				
$E_{\rm p,i}$ vs S	12	0.74	5.8×10^{-3}	0.408 ± 0.043	4.98 ± 0.22	0.496 ± 0.117	5.52 ± 0.62	0.135
$E_{{\rm p,i},z}$ vs $E_{\rm iso}$	12	0.83	9.5×10^{-4}	0.364 ± 0.030	-15.70 ± 1.53	0.266 ± 0.068	-10.61 ± 3.47	0.181
$E_{\rm p,p}$ vs $F_{\rm peak}$	12	0.54	7.1×10^{-2}	0.340 ± 0.045	4.39 ± 0.19	0.349 ± 0.161	4.52 ± 0.74	0.188
$E_{{\rm p,p},z}$ vs $L_{\rm iso}$	12	0.67	1.7×10^{-2}	0.396 ± 0.034	-17.68 ± 1.78	0.243 ± 0.078	-9.61 ± 4.07	0.200
				Type II GRBs				
$E_{\rm p,i}$ vs S	137	0.59	3.7×10^{-14}	0.418 ± 0.002	4.06 ± 0.01	0.295 ± 0.031	3.66 ± 0.14	0.227
$E_{{\rm p,i},z}$ vs $E_{\rm iso}$	137	0.70	1.4×10^{-21}	0.469 ± 0.003	-22.35 ± 0.14	0.338 ± 0.026	-15.27 ± 1.37	0.229
$E_{\rm p,p}$ vs $F_{\rm peak}$	136	0.58	2.2×10^{-13}	0.453 ± 0.004	4.68 ± 0.02	0.363 ± 0.041	4.31 ± 0.21	0.253
$E_{{\rm p,p},z}$ vs $L_{\rm iso}$	136	0.73	1.6×10^{-23}	0.494 ± 0.005	-23.32 ± 0.26	0.347 ± 0.029	-15.52 ± 1.51	0.251
				Type II GRBs with $t_{\rm jet}$ estimates				
$E_{{\rm p,i},z}$ vs $E_{\rm iso}$	30	0.82	4.1×10^{-08}	0.536 ± 0.004	-27.34 ± 0.21	0.418 ± 0.053	-19.62 ± 2.82	0.233
$E_{{\rm p,i},z}$ vs E_γ	30	0.76	1.1×10^{-06}	0.604 ± 0.008	-27.93 ± 0.42	0.499 ± 0.077	-22.69 ± 3.90	0.266
$E_{{\rm p,p},z}$ vs $L_{\rm iso}$	30	0.75	1.5×10^{-06}	0.529 ± 0.008	-25.12 ± 0.43	0.373 ± 0.063	-16.91 ± 3.30	0.282
$E_{{\rm p,p},z}$ vs L_γ	30	0.61	3.1×10^{-04}	0.731 ± 0.016	-33.87 ± 0.78	0.376 ± 0.097	-16.14 ± 4.86	0.343

Note. — N is the number of bursts in the fit sample, ρ_S is the Spearman correlation coefficient, P_{ρ_S} is the corresponding chance probability, a ($a_{\sigma_{\rm int}}$) and b ($b_{\sigma_{\rm int}}$) are the slope and the intercept for the fits without (with) intrinsic scatter $\sigma_{\rm int}$.

Selection effects

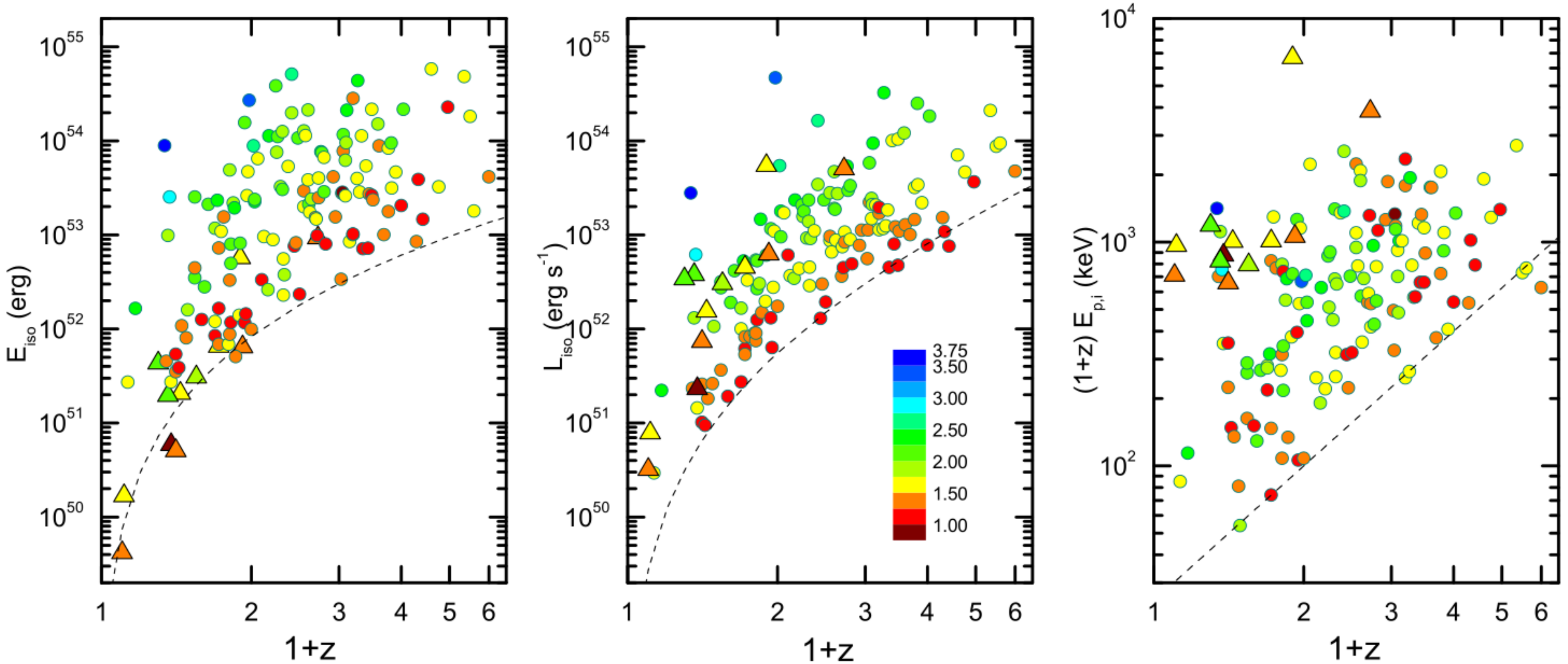

$S_{lim} \sim 3\times10^{-6}$ erg cm^{-2}

$F_{lim} \sim 1\times10^{-6}$ erg cm^{-2} s^{-1}

$E_{p,p,z} \sim 25(1+z)^2$ keV

GRB detection horizon

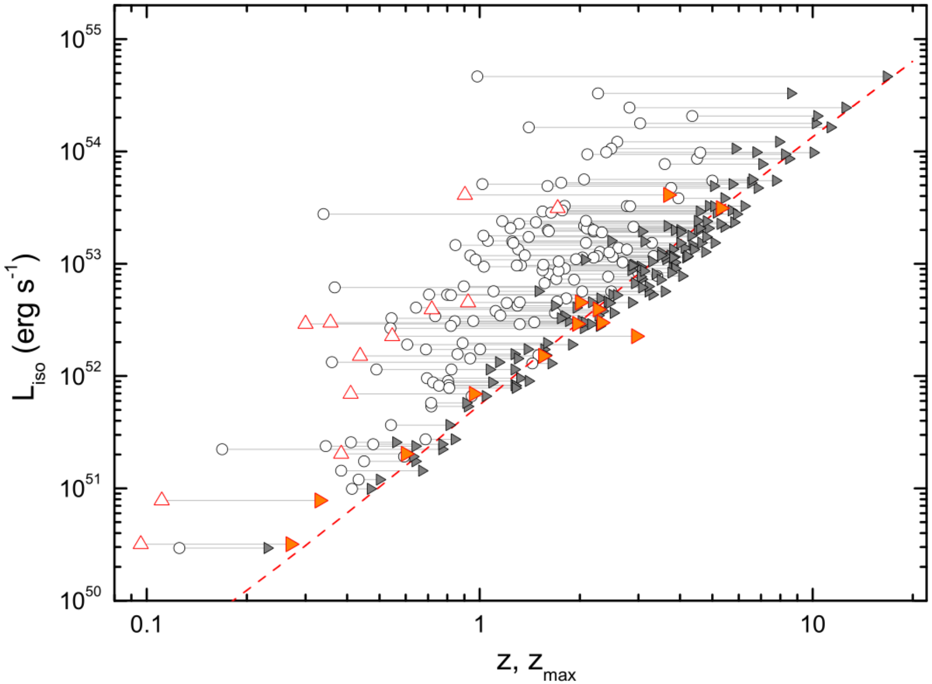

$F_{lim} = 1\times10^{-6}$ erg cm^{-2} s^{-1}

The highest z_{max}:

Type I

$z_{max} \sim 5.3$ for GRB 160410A ($z_0 = 1.72$)

Type II

$z_{max} \sim 16.6$ for GRB 110918A ($z_0 = 0.981$)

G2: ~80 – 300 keV

$$\mathrm{PCR}_z(\Delta T_{\mathrm{trig}}) = a \times \mathrm{PCR}_{z0}(a \cdot \Delta T_{\mathrm{trig}}) \times \frac{N_{\mathrm{G2}}(\alpha, \beta, a \cdot E_{\mathrm{p,p}})}{N_{\mathrm{G2}}(\alpha, \beta, E_{\mathrm{p,p}})} \times \left(\frac{D_{\mathrm{M}}(z_0)}{D_{\mathrm{M}}(z)}\right)^2$$

Trigger threshold: 9σ

Trigger time scales ΔT_{trig}: 140 ms or 1 s,

$a = (1+z_0)/(1+z)$,

$PCR_{z0}(a\Delta T_{trig})$ is reached in the observed G2 light curve on the modified time scale

$N_{G2}(\alpha,\beta,E_{pp})$ is the best spectral model count flux in G2 calculated using the DRM,

$N_{G2}(\alpha,\beta,aE_{pp})$ is the corresponding flux in the redshifted spectrum

Luminosity and energy release functions

Without loss of generality, the total luminosity function (LF; number of bursts per unit luminosity) $\Phi(L_{iso}, z)$ can be rewritten as

$$\Phi(L_{\rm iso}, z) \quad = \quad \rho(z)\phi(L_{\rm iso}/g(z), \alpha_s)/g(z)$$

Lloyd-Ronning (2002)

$\rho(z)$ – GRB formation rate (GRBFR)

$\phi(L_{\rm iso}/g(z))$ – local LF

$g(z) = (1+z)^{\delta}$ – luminosity evolution (Lloyd-Ronning 2002)

α_s – shape of the LF (Yonetoku 2004)

Non-parametric statistical technique: *Lynden-Bell (1971)* *Efron & Petrosian (1992)*

Examples of evolving astrophysical objects:

- Galaxies: the local luminosity function varies for early- and late-type galaxies (Marzke et al. 1994)
- Quasars: $L \sim (1+z)^3$, $z<1.5$ (Boyle 1993; Hewett, Foltz, & Chaffee 1993); $L \sim (1+z)^{1.5}$, $z<3$ (Hewett et al. 1993)

Selection effects and luminosity (energy release) evolution

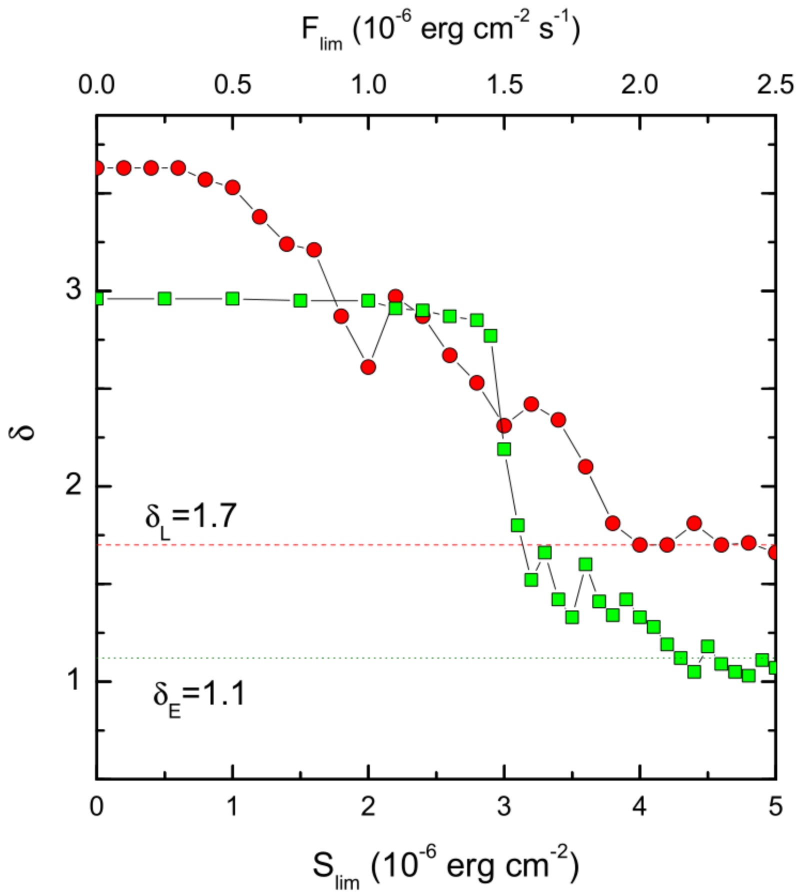

Red circles: Luminosity;
Green squares: Energy release.

$F_{lim} = 2 \times 10^{-6}$ erg cm^{-2} s^{-1} ;
$S_{lim} = 4.3 \times 10^{-6}$ erg cm^{-2} .

The present-time GRB luminosity and energy release functions

L_{iso}: τ_0 = 1.7 $\delta_L = 1.7^{+0.9}_{-0.9}$ (1σ CL)

E_{iso}: τ_0 = 1.6 $\delta_E = 1.1^{+1.5}_{-0.7}$

GRBs were brighter in the past

Cumulative luminosity function:

$$\ln \psi(L'_i) = \sum_{j=2}^{i} \ln\left(1 + \frac{1}{N'_j}\right)$$

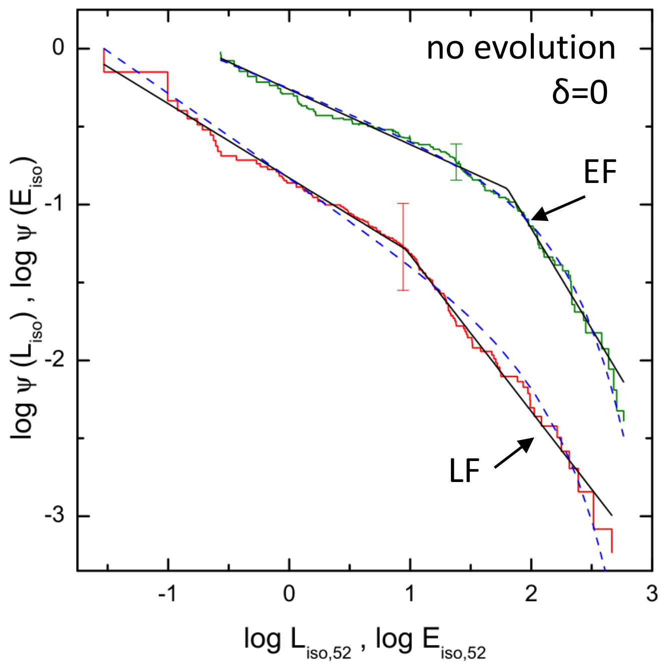

Best fit:
LF with BPL
($\alpha_1 \sim$ -0.5, $\alpha_2 \sim$ -1);
EF with CPL
(α ~ -0.3,
E_{cut} ~(2–4)×10^{54} erg).

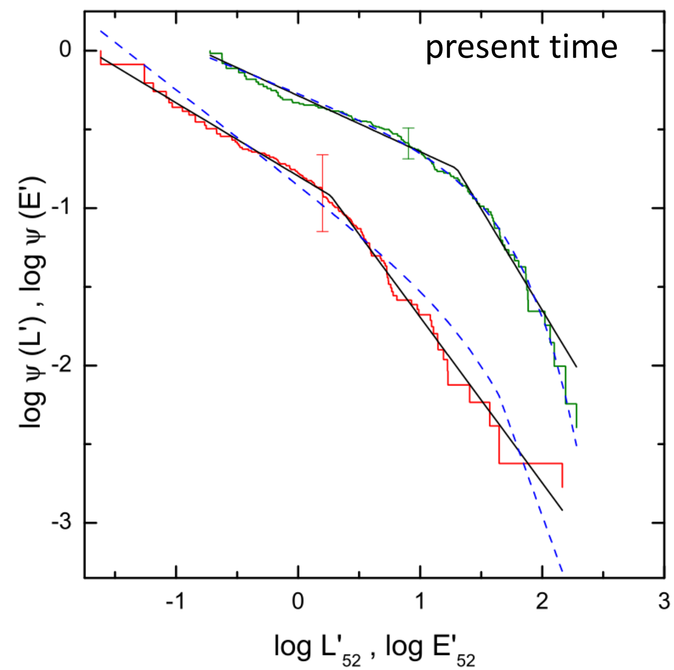

The existence of a sharp cutoff of the isotropic energy distribution of KW and *Fermi*/GBM GRBs around ~ 1−3×10^{54} erg was suggested recently by Atteia et al. (2017).

The present-time GRB luminosity and energy release functions

BPL:

$$\psi(x) \propto \begin{cases} x^{\alpha_1}, & x \leq x_b \\ x_b^{(\alpha_1-\alpha_2)} x^{\alpha_2}, & x > x_b \end{cases}$$

α_1, α_2 – PL indices at the dim and bright distribution segments,
x_b – breakpoint of the distribution.

CPL:

$$\psi(x) \propto x^{\alpha} \exp(-x/x_{\rm cut})$$

α – PL index,
x_{cut} – cutoff luminosity (or energy).

Data	Evolution (PL index)	Model	χ^2(d.o.f.)	α_1	α_2	$\log x_b$ ($\log x_{\rm cut}$)
$\psi(L')$	δ_L=1.7	BPL	2.05 (133)	-0.47 ± 0.06	-1.05 ± 0.11	0.27 ± 0.12
$\psi(L')$	δ_L=1.7	CPL	18.5 (134)	-0.60 ± 0.04		2.10 ± 0.15
$\psi(E')$	δ_E=1.1	BPL	19.2 (126)	-0.36 ± 0.01	-1.28 ± 0.11	1.30 ± 0.04
$\psi(E')$	δ_E=1.1	CPL	12.7 (127)	-0.31 ± 0.02		2.09 ± 0.04
$\psi(L_{\rm iso})$	no evolution	BPL	2.32 (133)	-0.47 ± 0.06	-1.00 ± 0.10	0.96 ± 0.15
$\psi(L_{\rm iso})$	no evolution	CPL	8.90 (134)	-0.54 ± 0.04		2.58 ± 0.11
$\psi(E_{\rm iso})$	no evolution	BPL	17.2 (126)	-0.35 ± 0.01	-1.29 ± 0.12	1.80 ± 0.05
$\psi(E_{\rm iso})$	no evolution	CPL	15.4 (127)	-0.32 ± 0.01		2.63 ± 0.04

GRB formation rate

The low-*z* GRBFR excess over SFR is in agreement with the results reported in Yu et al. (2015) and Petrosian et al. (2015).

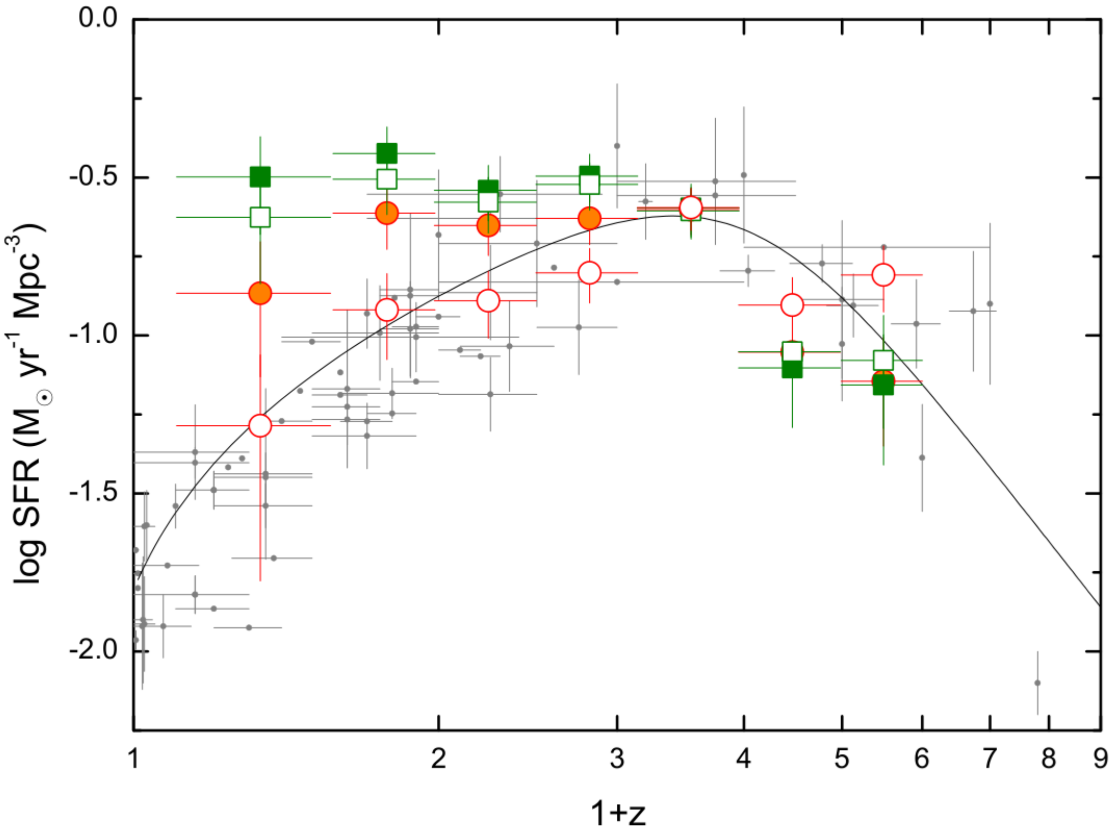

Cumulative rate evolution:

$$\ln \psi(z_i) = \sum_{j=2}^{i} \ln\left(1 + \frac{1}{M_j}\right)$$

Comoving density rate:

$$\rho(z) = \frac{d\psi}{dz}(1+z)\left(\frac{dV(z)}{dz}\right)^{-1}$$

Differential comoving volume:

$$\frac{dV(z)}{dz} = \frac{4\pi D_H D_M^2}{E(z)}$$

D_M is the transverse comoving distance

Hubble distance: $D_H = c/H_0$

Normalized Hubble parameter:

$$E(z) = \sqrt{\Omega_M(1+z)^3 + \Omega_\Lambda}$$

SFR: Hopkins (2004), Bouwens et al. (2011), Hanish et al. (2006), Thompson et al. (2006), Li (2008).

L_{iso}: red open circles: no luminosity evolution; red filled circles: $\delta_L = 1.7$;
E_{iso}: green open squares: no energy evolution; green filled squares: $\delta_E = 1.1$.

Summary

- A systematic study of 150 GRBs (from 1997 February to 2016 June) with known redshifts ($0.1 \le z \le 5$) was performed: 12 Type I (the merger-origin, typically short/hard) GRBs & 138 Type II (the collapsar-origin, typically long/soft) GRBs;
- Temporal analysis: burst durations & spectral lags;
- Spectral analysis with the CPL and Band functions;
- Energetics:
  - Observer-frame S and $F_{\rm peak}$ (10 keV–10 MeV);
  - Rest-frame $E_{\rm iso}$ and $L_{\rm iso}$;
  - Collimation-corrected E_γ and L_γ (for 32 GRBs with reasonably-constrained jet breaks).

Summary

- The “Amati” and “Yonetoku” correlations are confirmed for the KW sample;
- The correction for the jet collimation does not improve the “Amati” and “Yonetoku” correlations for the KW sample;
- The influence of instrumental selection: the regions above the limits, corresponding to the bolometric fluence $S_{lim} \sim 3\times10^{-6}$ erg cm^{-2} (in the E_{iso} – z plane) and bolometric peak energy flux $F_{lim} \sim 1\times10^{-6}$ erg cm^{-2} s^{-1} (in the L_{iso} – z plane) may be considered free from the selection biases;
- KW GRB detection horizon: Type I: z_{max}=5.3, Type II: $z_{max} \sim 16.6$, stressing the importance of GRBs as probes of the early Universe;
- The GRB luminosity evolution (is present @ $\sim1.6\sigma$,), LF and EF, and the evolution of the GRBFR were estimated accounting for the instrumental bias;
- The derived GRBFR features an excess over the SFR at $z < 1$ and nearly traces the SFR at higher redshifts.

Thank you!

The talk is based on the paper Tsvetkova, Frederiks, Golenetskii et al., ApJ accepted

tsvetkova@mail.ioffe.ru